Nanoscale

PAPER

View Article Online
View Journal | View Issue

Cite this: *Nanoscale*, 2021, **13**, 14417

A nanoparticle-containing polycaprolactone implant for combating post-resection breast cancer recurrence

Yu Gao, †[a] Jiahui Wang,†[a] Hao Han,†[b] Huaxin Xiao,[a] Wei-kui Jin,[b] Siyu Wang,[a] Shengpei Shao,[a] Zhixuan Wang,[c] Wenjing Yang, [a] Lianhui Wang [a] and Lixing Weng*[a,c]

The recurrence and metastasis of tumor after surgery is the main cause of death for patients with breast cancer. Systemic chemotherapy suffered from low delivery efficiency to tumors and the side effects of chemo drugs. Localized chemotherapy using drug-containing implants is an alternative, while the reconstruction of breast tissue is generally considered after chemotherapy, resulting in a second surgery for patients. Here, we describe a strategy using implantable drug-containing polymeric scaffolds to deliver chemo drugs directly to the post-resection site, and simultaneously provide mechanical support and regenerative niche for breast tissue reconstruction. When doxorubicin was loaded in mesoporous silica nanoparticles and subsequently incorporated into polycaprolactone scaffolds (DMSN@PCL), a 9-week sustained drug release was achieved post implantation in mice. The local recurrence of residual tumor after surgery was significantly inhibited within 4 weeks in a post-surgical mouse model bearing xenograft MDA-MB-231 tumor. DMSN@PCL scaffolds exhibited good biocompatibility in mice during the treatment. We believe our strategy holds great promise as an adjuvant localized chemotherapy in clinics for combating post-resection breast cancer recurrence.

Received 25th June 2021,
Accepted 2nd August 2021

DOI: 10.1039/d1nr04125h

rsc.li/nanoscale

Introduction

Breast cancer is the most commonly diagnosed cancer (24.5%) and the leading cause (15.5%) of cancer death for women worldwide.[1] It contains three major subtypes including hormone receptor (*e.g.* estrogen or progesterone) positive/human epidermal growth factor 2 (HER2) negative, HER2 positive, and triple-negative (TNBC). Surgery, referred to as a total mastectomy or an excision, is often the standard treatment for nonmetastatic breast cancer.[2] However, the 10-year risk of the recurrence was up to 35% in women who received breast-conserving surgery only.[3] In particular, TNBC is more likely to recur than the other two subtypes due to its nature of aggressive proliferation. Therefore, a systemic chemotherapy after surgery is usually performed for combating the recurrence.[4] To improve the survival and quality of life, targeting nanoparticles were applied by increasing the bioavailability and solubility of drugs, with the aim of achieving high therapeutic concentrations of chemotherapy at the site of tumors.[5–9] However, only 0.7% (median) of the administrated nanomedicine was delivered to a solid tumor, resulting in limited therapeutic efficacy and unwanted side effects.[10] More efficient localized chemotherapy for patients with nonmetastatic TNBC is of great importance for both suppressing the recurrence and reducing patient morbidity.[11,12]

Drug-loaded implants can be applied directly to the site of resection, offering localized and prolonged drug release with minimal side effects caused by systemic administration. Implants made by biodegradable polymers provide a one-time administration of drugs without the need of removal by a second surgery, thereby attracting more and more attention in clinical settings.[13–15] For example, Gliadel® Wafer made by carmustine-containing polyanhydride improves long-term survival among patients diagnosed with aggressive gliomas.[16] The improved therapeutic efficacy might be attributed to the localized and sustained release of drugs, enabling a prolonged exposure of tumor cells to chemotherapy over multiple cell cycles, which has been proved to be more cytotoxic than most

[a]*State Key Laboratory for Organic Electronics and Information Displays & Jiangsu Key Laboratory for Biosensors, Institute of Advanced Materials (IAM), Jiangsu National Synergistic Innovation Center for Advanced Materials (SICAM), Nanjing University of Posts and Telecommunications, 9 Wenyuan Road, Nanjing 210023, China. E-mail: lxweng@njupt.edu.cn*
[b]*Department of Ultrasound, Nanjing Drum Tower Hospital, The Affiliated Hospital of Nanjing University Medical School, Nanjing 210008, China*
[c]*School of Geography and Biological Information, Nanjing University of Posts and Telecommunications, 9 Wenyuan Road, Nanjing 210023, China*
†These authors contributed equally.

systemic administrated drugs that disrupt cell replication.[13] Moreover, considering the need of breast tissue reconstruction for patients with mastectomy or excision, drug-loaded implants with the ability to provide mechanical support and to improve soft tissue regeneration may be promising as an adjuvant therapy for nonmetastatic TNBC.

Polycaprolactone (PCL) is a well-investigated biomaterial and has been used as a scaffold for bone regeneration in clinics.[17] PCL is an aliphatic polyester with a semicrystalline structure, low glass transition temperature (60 °C), and highly flexible mechanical properties. Owing to its slow degradation in tissue and the compatibility with various drugs, sustained release of anticancer drugs for several months has been achieved in vitro.[15] The biodegradable and biocompatible properties of PCL make it particularly applicable as an implant with minimal concern for fibrosis and inflammation. Unlike the traditional silicone implant for breast reconstruction, PCL supresses fibrous capsule formation that results in capsular contraction.[18] Thereby, PCL represents a new generation of biomaterial for scaffolds that not only provide localized chemotherapy but also facilitate post-surgical breast reconstruction. Previously, we have demonstrated the growth inhibition of cancer cells on a doxorubicin-containing silica-nanoparticle/PCL nanocomposite (DMSN@PCL) film fabricated by the cryomilling method.[19] In the present work, we aim to investigate the drug release and the effect against recurrence of the DMSN@PCL scaffolds in a post-surgical mouse model bearing xenograft breast tumor. A sustained and localized release of doxorubicin *in vivo* for more than 9 weeks was observed, which resulted in significant inhibition of local recurrence of breast tumor after resection.

Experimental

Materials, cells and animals

Mesoporous silica nanoparticles (MSN), polycaprolactone (PCL), polyvinyl alcohol (PVA), doxorubicin (Dox) and sodium chloride (NaCl) were purchased from Sigma-Aldrich. The fluorescent dye cyanine 5.5 (Cy5.5) was purchased from Beijing Fanbo Biochemicals Co. Ltd. D-Luciferin potassium salt was purchased from Shanghai Yeasen Biotech Co. Ltd. MDA-MB-231 and luciferase-tagged MDA-MB-231 breast cancer cells were purchased from Shanghai Bang Yao Biological Technology Co. Ltd. Female BALB/c nude mice (4–6 weeks) were obtained from Nanjing Qinglong Mountain Animal Breeding Field. All animal procedures were performed in accordance with the Guidelines for Care and Use of Laboratory Animals of Nanjing Drum Tower Hospital and approved by the Animal Ethics Committee of Nanjing Drum Tower Hospital, The Affiliated Hospital of Nanjing University Medical School.

Preparation of DMSN@PCL scaffolds

To load Dox into the MSNs, 5 mL of Dox solution (0.5 mg mL^{-1}) was mixed with 5 mg of MSNs and stirred for 12 h. Then the mixed solution was centrifuged for 20 min at a speed of 8000 rpm. After centrifugation, DMSN was frozen in a refrigerator (−4 °C) for 1 h, and then lyophilized for 24 h. The loading efficiency of Dox was determined to be 9.83% by quantification of the absorbance at 575 nm.

To prepare DMSN@PCL scaffolds, PCL and DMSNs were mixed at the ratio of 1 : 20, 1 : 100, and 1 : 1000, respectively. Sodium chloride powders (5%) were added to the mixture. The mixture was cryomilled and then heated (80 °C) in wafer molds to form the scaffolds. After cooling, the DMSN@PCL scaffolds were immersed in water for 12 h to dissolve the sodium chloride.

Characterization

The morphology and drug distribution of DMSN@PCL scaffolds were studied using a scanning electron microscope (E-1010/S4800, Japan) and an FV1000 laser scanning confocal microscope (Olympus, Japan). The mechanical properties were tested using a CMT6502 universal testing machine (MTS, China), at a speed of 3 mm per minute. Triplicates of each sample were performed.

Drug release profile

All the samples were placed in a 24-well plate and 1 mL of phosphate buffer solution (PBS, pH 7.4) were added into each well. The solutions in each well were collected at predetermined time points for the quantification of released Dox, and 1 mL of PBS were replenished to each well. Triplicates of each sample were performed.

To study the *in vivo* release profiles of Dox, DMSN@PCL scaffolds containing Cy5.5 were surgically implanted into mice. For the control group, the same amount of Cy5.5 was subcutaneously injected into mice. Then the mice were imaged using an *in vivo* imaging system (IVIS Lumina K Series III, PerkinElmer).

Inhibition of cell viability *in vitro*

MDA-MB-231 breast cancer cells were incubated at 37 °C with 5% CO_2 and cultured in L-15 medium with 10% fetal bovine serum and 1% penicillin/streptomycin. Cells were seeded into Transwell plates (24-well) with a density of 5×10^4 and allowed for attachment. Then PBS, PCL, free Dox (2.5 μg mL^{-1}) and 5% DMSN@PCL scaffolds (2.5 μg mL^{-1} Dox) were added to the inner well of each group, respectively. All treatments were applied on day 0. Then the cells were cultured for 8 days and the medium was replaced once every two days. The cell viability at predetermined time points was tested by MTT assay. Triplicates of each sample were performed.

Inhibition of tumor growth *in vivo*

Luciferase-tagged MDA-MB-231 cells (1×10^7) suspended in 50 μL of PBS were subcutaneously injected into each BALB/c nude mouse. When the tumors reached an approximate size of 100 mm^3, the mice were randomly divided into four groups. Then the tumors were resected, leaving 5% residual tumor tissue in the surgical bed. The PCL or DMSN@PCL (5% of DMSN) scaffolds were implanted at the resection site. The

wounds of all mice were closed by suture. For untreated and free Dox treated groups, saline or 2.5 μg of Dox were administrated by tail vein injection. During the experiment, the growth of each tumor was monitored weekly using an *in vivo* imaging system. The survival rate and the body weight of the mice were recorded. After 4 weeks, all the mice were euthanized, and the tissues including the heart, liver, spleen, lungs, kidneys, and tumor were collected. Histological analysis was performed by hematoxylin–eosin (H&E) staining. The tissues at the site of implantation were collected for H&E staining.

Statistical analysis

All data were expressed as mean ± SD. Inter- and intragroup comparisons and analysis in each experiment were performed by the unpaired Student's *t* test and one-way analysis of variance (ANOVA) using SPSS software. Probability (*P*) values of <0.05 were considered statistically significant.

Results and discussion

Mesoporous silica nanoparticles (MSNs), known to improve the bioavailability and overcome the drug resistance through efficient cellular uptake and *P*-glycoprotein inhibition, were used to encapsulate the chemotherapy drug, *i.e.* doxorubicin (Dox).[20] Dox was loaded by physical adsorption within the pores of MSNs with a drug loading efficiency of 9.83% (DMSN). The porosity and pore size of the PCL scaffold not only influence the drug release kinetics but also the host biological responses such as host cell infiltration and vascular ingrowth.[21] In order to generate micropores throughout the scaffolds, a mixed powder of NaCl, PCL, and DMSN was cryomilled and then heated in wafer molds to form DMSN@PCL scaffolds with a diameter of 6 mm and a thickness of 2 mm (Fig. 1A). Cryomilling not only preserved the drug activity but also facilitated the homogeneous distribution of DMSN within the DMSN@PCL scaffolds (Fig. 1B and C), which is in good agreement with reported work.[22] After being immersed in water, NaCl powders were dissolved, resulting in micropore formation. Under a scanning electrical microscope, plain PCL scaffolds exhibited a featureless morphology, whereas the NaCl generated micro-sized pores after being dissolved in water (Fig. 1D). DMSNs appeared on the surface or within the pores as expected, suggesting the successful integration of inorganic nanoparticles within the polymer matrix.

As the scaffolds should be able to withstand the subcutaneous pressure (slightly higher than the standard atmospheric pressure) after implantation, and their mechanical properties should be similar to those of the breast tissue, we next studied the mechanical properties of DMSN@PCL scaffolds by compression tests (Fig. 2A). The representative stress–strain curves are depicted in Fig. 2B. As shown in Fig. 2, the micropores generated by NaCl ingredient resulted in decreased

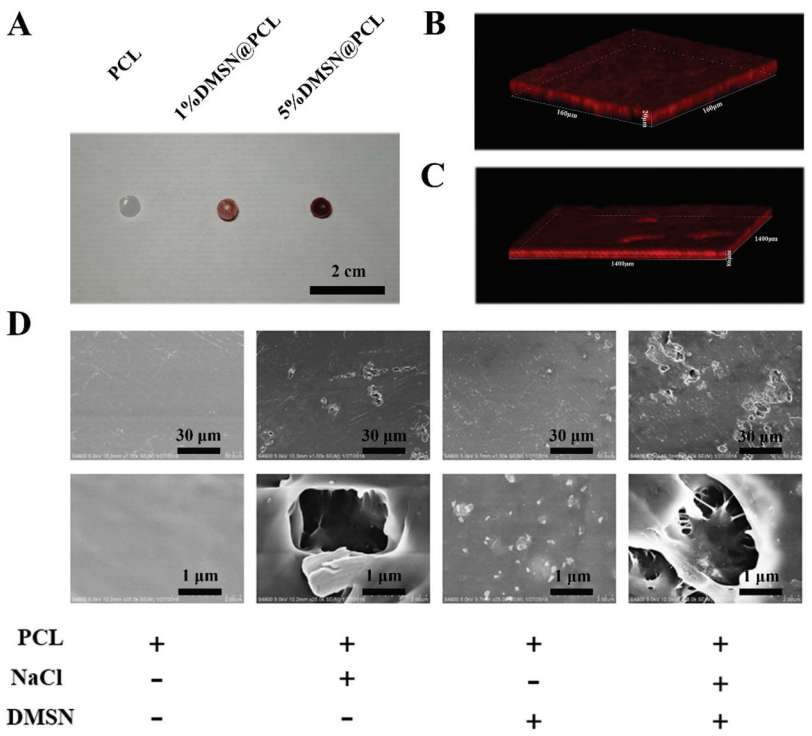

Fig. 1 Characterization of the DMSN@PCL scaffolds. (A) Images of the plain PCL and DMSN@PCL scaffolds (1% and 5% of DMSN); (B) confocal scanning of the DMSN@PCL scaffolds without NaCl (160 × 160 × 20 μm) and (C) DMSN@PCL scaffolds with NaCl (1400 × 1400 × 86 μm); (D) SEM images of PCL, PCL with NaCl, DMSN@PCL without NaCl, and DMSN@PCL with NaCl.

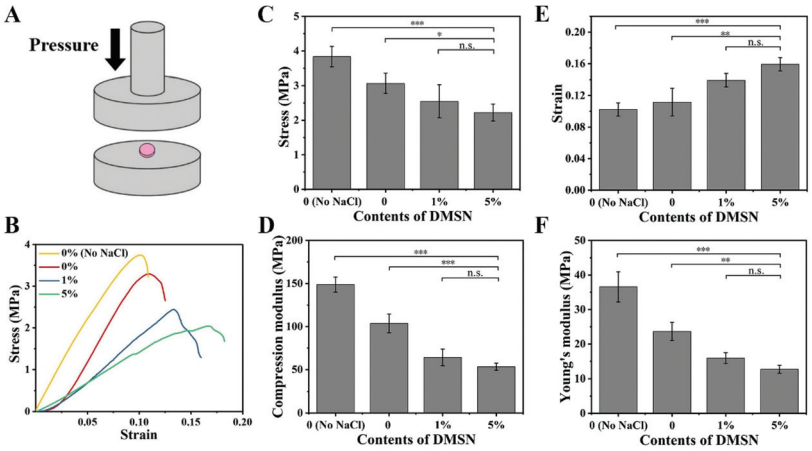

Fig. 2 Characterization of the mechanical properties of the DMSN@PCL scaffolds. (A) Schematic illustration of the mechanical test; (B) stress–strain curves of the PCL without NaCl (0% no NaCl), PCL with NaCl (0%) and DMSN@PCL (1% and 5% of DMSN); (C) stress, (D) compression modulus, (E) strain, and (F) Young's modulus of the above tested scaffolds (n = 3). *, **, and *** indicate $p < 0.05$, 0.01, and 0.001, respectively; n.s. indicates $p > 0.05$ (no significance).

mechanical properties including stress (Fig. 2C), compression modulus (Fig. 2D) and Young's modulus (Fig. 2F). These values further decreased with the integration of DMSN, due to the interruption of the interconnected polymer chains. In contrast, the values of strain were increased with the increase of DMSN concentrations (Fig. 2D), which might be attributed to the incorporation of inorganic nanoparticles into the polymeric matrix. The compression modulus and Young's modulus were 58.7 and 16.6 MPa for DMSN@PCL with 1% DMSN, and 46.7 and 12.9 MPa for DMSN@PCL with 5% DMSN, respectively. These values were much higher than the standard atmospheric pressure (101.3 kPa) and were similar to the strength of the breast tissue, which ranges from 0.4 to 40 MPa according to the literature.[23] It should be noted that a higher percent of DMSN (*i.e.* 30%) significantly compromised the mechanical properties of the DMSN@PCL scaffold which even immediately collapsed after heat molding. Thus, DMSN@PCL scaffolds with the percent of DMSN below 5% are applicable for breast tissue post-surgical implantation.

The median duration of the adjuvant chemotherapy for TNBC ranged from 2 to 4 months. Therefore, a prolonged release profile of the DMSN@PCL scaffold is favourable for post-surgical chemotherapy. As shown in Fig. 3A, a burst release and then a sustained release of Dox form the PCL matrix were observed and the cumulative release reached a plateau after 10 days, accounting for 48.0% of the loaded Dox (0.1% Dox@PCL). Once being encapsulated by MSNs, the equivalent amount of Dox exhibited a retarded release profile by 1% DMSN@PCL scaffolds, reaching the plateau (40.0%) after 50 days. An increase of the concentration of DMSN will not change the release profile, as a similar plot was shown by 5% DMSN@PCL to that by 1% DMSN@PCL. The cumulative Dox release of 5% DMSN@PCL after 50 days in PBS was 42%. Thus, the DMSN@PCL scaffold showed a burst Dox release within 24 hours, followed by a four-week sustained release and a small amount of Dox release until 8 weeks *in vitro*. As PCL hardly degraded in PBS at room temperature, 100% release of Dox cannot be achieved in the *in vitro* experiment. A further

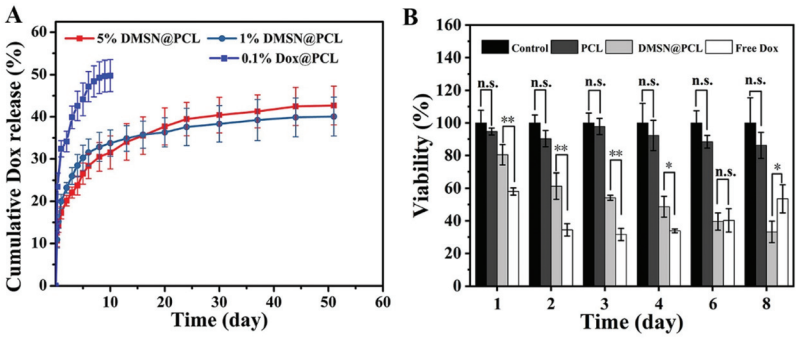

Fig. 3 The drug release profile and the inhibition of cancer cell viability *in vitro* by DMSN@PCL scaffolds. (A) Cumulative Dox release of the DMSN@PCL scaffolds with different contents of DMSN. (B) The viability of MDA-MB-231 cells incubated with culture medium (control), PCL, DMSN@PCL (5% of DMSN), and free Dox over 8 days (n = 3). * and ** indicate $p < 0.05$ and 0.01, respectively; n.s. indicates $p > 0.05$ (no significance).

release will be expected when the degradation of PCL happened. These findings were in good agreement with the release profile of the tissue-engineered PCL-chitosan scaffold for inhibition of bone metastasis.[24]

We next set to investigate the inhibition of cancer cell viability by DMSN@PCL scaffolds in an *in vitro* assay. The MDA-MB-231 cell line was used to evaluate the anti-TNBC efficiency. Cells were cultured and allowed to be attached in a Transwell plate (24-well), and all treatments were applied to the inner well of each group on day 0. Then the cells were cultured for 8 days and the medium was replaced once every two days. As shown in Fig. 3B, free Dox (2.5 μg mL^{-1}) exhibited a viability inhibition of 34.5% on day 2, and this effect remained at 31.6% and 33.8% on day 3 and day 4, respectively. As the culture medium was replaced (to mimic the clearance), then the cell viability increased to 40.3% and 53.5% on days 6 and 8, respectively, suggesting the regrowth of MDA-MB-231 cells after treatment. When treated with 5% DMSN@PCL (2.5 μg mL^{-1} Dox), the viability of cells gradually decreased with time. The viability was 61.0% on day 2 by DMSN@PCL, while it decreased to 34.5% on day 8, suggesting the successful inhibition of the growth of MDA-MB-231 cells for 8 days. There were no significant differences of the viability between the PCL treated group and the control group, demonstrating the good biocompatibility of PCL scaffolds.

Then the drug release of DMSN@PCL was studied in a mouse model. Dox was replaced by Cy5.5, which was then subcutaneously injected (Cy5.5) or implanted (DMSN@PCL) into the mice. To confirm the fluorescence stability of Cy 5.5, a tube of Cy 5.5 solution was imaged daily using an animal imaging system for 8 days, and the fluorescence intensities were quantified. There was no significant difference of the fluorescence intensities for 8-day observation (data not shown). The fluorescence intensity of subcutaneously injected Cy5.5 decreased rapidly within 4 hours (17.8%), and the fluorescence was undetectable after 24 hours post treatment, suggesting the fast kinetics of drug clearance through subcutaneous injection (Fig. 4A and C). In contrast, the fluorescence intensity of loaded Cy5.5 gradually decreased within 9 weeks, suggesting a sustained drug release from DMSN@PCL scaffolds *in vivo* (Fig. 4B and D). The DMSN@PCL scaffolds served as drug depots after implantation, replenishing the active drug to surrounding tissues against clearance, and therefore maintaining the therapeutic concentration for a relatively long period. The fluorescence intensity of DMSN@PCL scaffolds decreased to 55.9% after 9 weeks post implantation; in other words, a release of 44.1% of loaded drugs was achieved. A further release can be expected due to the degradation of PCL progressing in the body, which usually takes more than a year for noticeable degradation and up to four years for total degradation.[25] It is worth noting that the degradation kinetics of PCL scaffolds prolonged the duration time of adjuvant chemotherapy for post-surgical breast cancer.

The inhibition of tumor recurrence by DMSN@PCL scaffolds was then evaluated by a post-surgical mouse model bearing MDA-MB-231 tumor xenograft. Luciferase labelled MDA-MB-231 was subcutaneously injected into the BALB/c nude mice. When all the tumors reached approximately 100 mm^3 in volume, the mice were randomly divided into four groups, followed by resection of 95% of each tumor. Then the mice were subjected to different treatments, *i.e.* intravenous

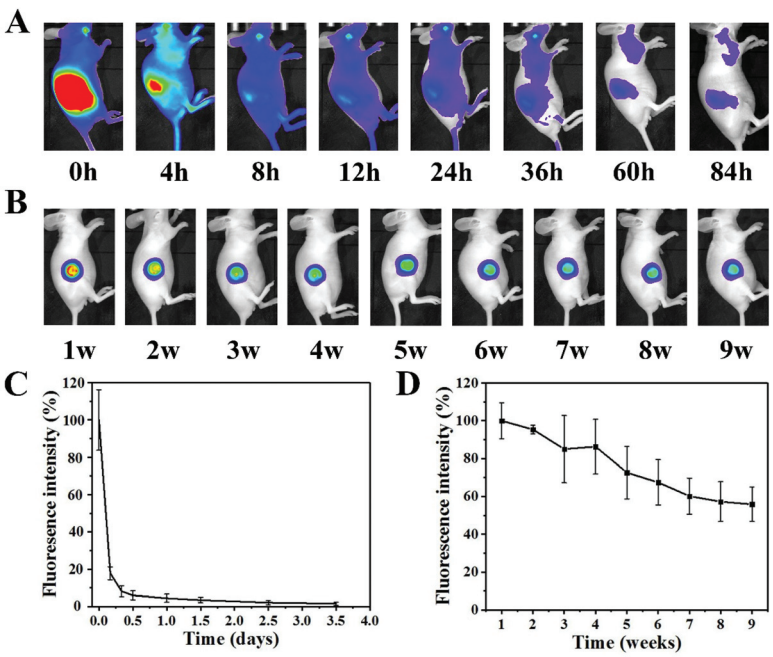

Fig. 4 *In vivo* drug release profiles from DMSN@PCL scaffolds. (A) Representative fluorescence images of subcutaneously injected Cy5.5 and (B) Cy5.5 loaded into DMSN@PCL scaffolds at different times. (C) Quantification of the fluorescence intensities of subcutaneously injected Cy5.5 and (D) Cy5.5 loaded into DMSN@PCL scaffolds (n = 3).

injection of saline (untreated) or 2.5 μg of Dox (free Dox), and implantation of PCL scaffolds (PCL) or DMSN@PCL scaffolds (containing 2.5 μg of Dox), respectively. After treatments, the wound sites were closed by suture, and the tumor regrowth was monitored by bioluminescence imaging. As shown in Fig. 5A and B, the residual tumors started to grow in one week post-treatment, including the groups treated with saline, free Dox, and PCL scaffolds. Then the tumors in these groups gradually progressed, resulting in tumor regrowth and even deaths of mice within four weeks. In contrast, the growth of residual tumors was supressed by the DMSN@PCL scaffolds, indicating the ability to combat local recurrence. The weight measurements of the tumors collected after 4 weeks supported the results observed in bioluminescence imaging. Therefore, DMSN@PCL scaffolds supressed the tumor regrowth within 4 weeks, which might be attributed to the continuous release of DMSN from the scaffolds, resulting in sustained growth inhibition of residual MDA-MB-231 cells, similar to the effect in the *in vitro* assay.

During treatment, the DMSN@PCL scaffolds exhibited good biocompatibility in mice after implantation. As shown in Fig. 6A, there was no significant difference between the average weights of all the mice within 28 days. All the plots slightly decreased after surgery, and then started to increase as normal. The survival of mice treated with saline, free Dox, and PCL was 40%, 20%, and 40%, respectively, due to the recurrence of the tumor. None of the mice died within 28 days by the treatment of DMSN@PCL scaffolds (Fig. 6B), suggesting both the good therapeutic efficacy and good biocompatibility. The histological analysis of the main organs collected from the mice 4 weeks post treatment revealed no harmful injury in all tested groups except the spleen sample in the free Dox treated group (Fig. 6C). Blurred boundaries of the spleen sample were observed in the histological image of the free Dox treated group. Doxorubicin will facilitate splenic contraction *via* the mechanisms including intoxicated splenic macrophages, oxidative stress and mitochondrial dysfunction.[26] In the present study, the dosage of Dox was 2.5 μg per scaffold, which was much lower than the dosage in the literature. Such a low dosage can effectively inhibit the regrowth of tumor cells after resection, which might be attributed to the high delivery efficiency of DMSN@PCL scaffolds.[27] It was found that there was no observable ulcer, erosion, and necrosis of the tissue adjacent to the implanted scaffolds (Fig. 7), while an increase of immune cell infiltration was present compared to the non-

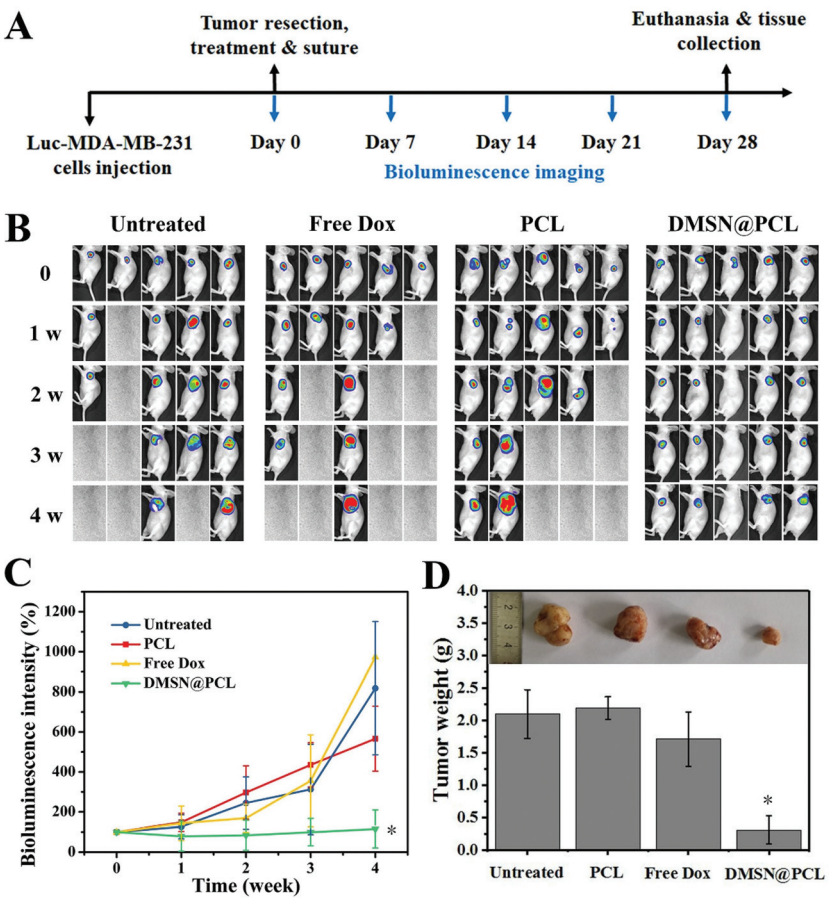

Fig. 5 DMSN@PCL scaffolds effectively inhibit the post-surgical recurrence. (A) Schematic illustration of the treatment schedule. (B) Representative bioluminescence images of the MDA-MB-231 tumors after different treatments as indicated. (C) Quantification of the bioluminescence intensities in A (n = 5). (D) Average tumor weight of mice after different treatments (n = 5). * indicates $p < 0.05$.

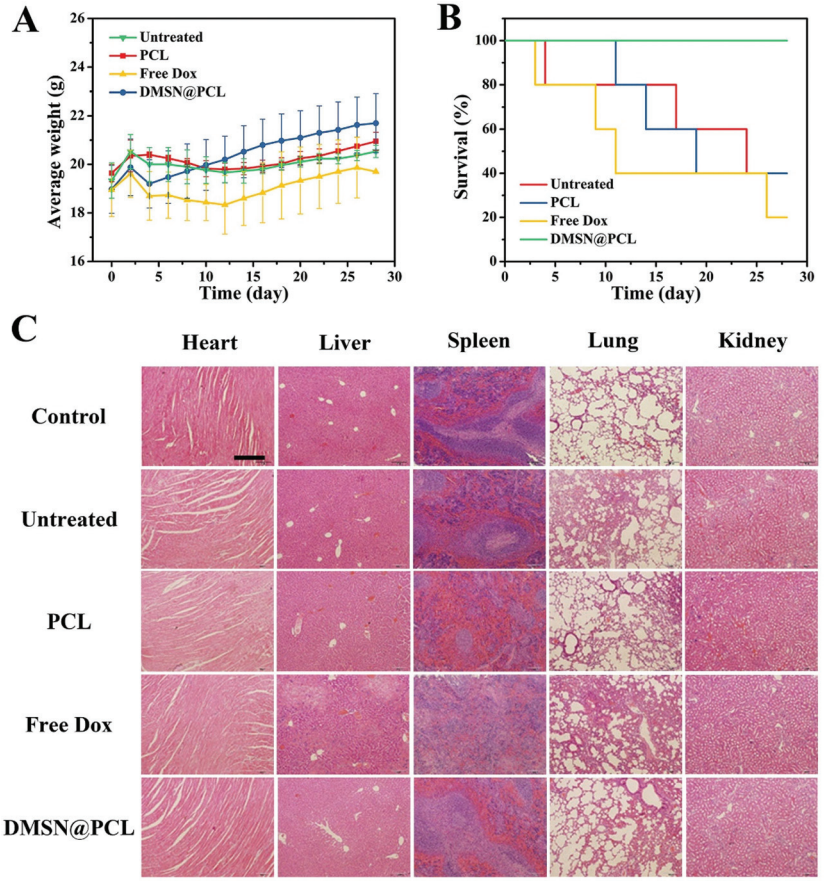

Fig. 6 DMSN@PCL scaffolds exhibited good biocompatibility in mice. (A) The average body weight and (B) the survival curve of mice after different treatments as indicated (n = 5). (C) Histological analysis of the major organs (heart, liver, spleen, lungs, and kidneys) collected from the mice with different treatments for 4 weeks. Scale bar: 200 μm.

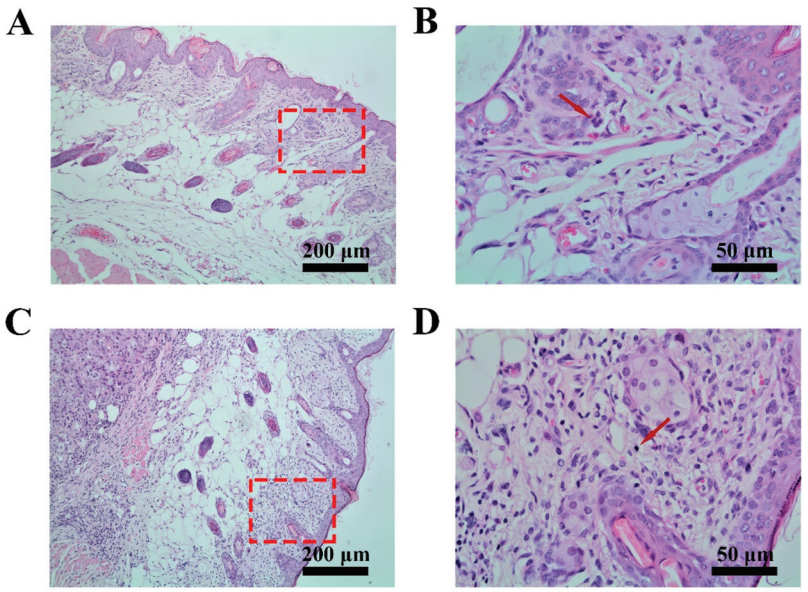

Fig. 7 Absence of ulcer, erosion, and necrosis of the tissue adjacent to the DMSN@PCL scaffolds. (A) H&E staining of the tissue at the wound site without any treatment after 28 days. (B) Enlarged image of the indicated area in A. (C) H&E staining of the tissue adjacent to the DMSN@PCL scaffolds 28 days post implantation. (D) Enlarged image of the indicated area in C. Red arrows indicate the immune cells.

implantation group. These results suggested a good biocompatibility of DMSN@PCL scaffolds in mice after implantation.

Conclusions

In conclusion, DMSN@PCL scaffolds provide an alternative adjuvant local chemotherapy for post-surgical TNBC, not only preventing the local recurrence but also offering necessary mechanical support for breast tissue reconstruction. Although a 9-week sustained drug release of DMSN@PCL scaffolds was demonstrated in mice, the release kinetics and periods can be further adjusted by optimizing the amounts of incorporated DMSN and the porosity of the DMSN@PCL scaffolds, personalizing the treatment of TNBC for individuals. After the adjuvant chemotherapy, the mechanical support and the regenerative niche provided by the DMSN@PCL scaffolds will facilitate the breast tissue reconstruction, with minimal concern for side effects, implant rupture, and immune rejection. Given the importance of local delivery of chemo drugs and breast tissue reconstruction, we believe our strategy holds great promise as an adjuvant chemotherapy in clinics for combating TNBC post-resection recurrence.

Author contributions

Y. G. and L. X. W. designed the study. Y. G., J. H. W., H. X. X., S. Y. W., S. P. S., and Z. X. W. carried out synthesis, characterization and all *in vitro* assays. J. H. W. and H. H. performed the animal experiments. W. K. J. and W. J. Y. helped and gave valuable suggestions for the animal experiments. Y. G., L. H. W. and L. X. W. wrote the manuscript. All authors discussed the results and commented on the manuscript.

Conflicts of interest

There are no conflicts to declare.

Acknowledgements

This work was supported by the National Key Research and Development Program of China (2017YFA0205302, 2017YFA0205301), Jiangsu Provincial Key Research and Development Program (BE2018732), Natural Science Foundation of Jiangsu Province (BK20180089), and the Priority Academic Program Development of Jiangsu Higher Education Institutions (PAPD, YX030003), the open research fund of Jiangsu Key Laboratory for Biosensors (51204080).

Notes and references

1 H. Sung, J. Ferlay, R. L. Siegel, M. Laversanne, I. Soerjomataram, A. Jemal and F. Bray, *CA-Cancer J. Clin.*, 2021, **71**, 209–249.
2 N. Harbeck and M. Gnant, *Lancet*, 2017, **389**, 1134–1150.
3 S. Darby, P. McGale and C. Correa, *Lancet*, 2011, **378**, 1707–1716.
4 A. G. Waks and E. P. Winer, *J. Am. Med. Assoc.*, 2019, **321**, 288–300.
5 M. J. Mitchell, M. M. Billingsley, R. M. Haley, M. E. Wechsler, N. A. Peppas and R. Langer, *Nat. Rev. Drug Discovery*, 2021, **20**, 101–124.
6 S. Wang, X. Guo, W. Xiu, Y. Liu, L. Ren, H. Xiao, F. Yang, Y. Gao, C. Xu and L. Wang, *Sci. Adv.*, 2020, **6**, eaaz8204.
7 S. Wang, X. Guo, L. Ren, B. Wang, L. Hou, H. Zhou, Q. Gao, Y. Gao and L. Wang, *Ultrason. Sonochem.*, 2020, **67**, 105188.
8 Y. Gao, C. U. Chan, Q. Gu, X. Lin, W. Zhang, D. C. L. Yeo, A. M. Alsema, M. Arora, M. S. K. Chong, P. Shi, C.-D. Ohl and C. Xu, *NPG Asia Mater.*, 2016, **8**, e260–e260.
9 C. Xu and K. Pu, *Chem. Soc. Rev.*, 2021, **50**, 1111–1137.
10 S. Wilhelm, A. J. Tavares, Q. Dai, S. Ohta, J. Audet, H. F. Dvorak and W. C. W. Chan, *Nat. Rev. Mater.*, 2016, **1**, 16014.
11 C. Zhang, Z. Zeng, D. Cui, S. He, Y. Jiang, J. Li, J. Huang and K. Pu, *Nat. Commun.*, 2021, **12**, 2934.
12 Z. Zeng, C. Zhang, J. Li, D. Cui, Y. Jiang and K. Pu, *Adv. Mater.*, 2021, **33**, 2007247.
13 J. B. Wolinsky, Y. L. Colson and M. W. Grinstaff, *J. Controlled Release*, 2012, **159**, 14–26.
14 Y. Gao, J. Lim, S.-H. Teoh and C. Xu, *Chem. Soc. Rev.*, 2015, **44**, 6306–6329.
15 S. Talebian, J. Foroughi, S. J. Wade, K. L. Vine, A. Dolatshahi-Pirouz, M. Mehrali, J. Conde and G. G. Wallace, *Adv. Mater.*, 2018, **30**, 1706665.
16 A. Bregy, A. H. Shah, M. V. Diaz, H. E. Pierce, P. L. Ames, D. Diaz and R. J. Komotar, *Expert Rev. Anticancer Ther.*, 2013, **13**, 1453–1461.
17 Y. Liu, J. Lim and S.-H. Teoh, *Biotechnol. Adv.*, 2013, **31**, 688–705.
18 L. Luo, Y. He, Q. Chang, G. Xie, W. Zhan, X. Wang, T. Zhou, M. Xing and F. Lu, *Int. J. Nanomed.*, 2016, **11**, 6471–6483.
19 Y. Gao, J. Lim, Y. Han, L. Wang, M. S. K. Chong, S.-H. Teoh and C. Xu, *Nanoscale*, 2016, **8**, 2568–2574.
20 Y. Gao, Y. Chen, X. Ji, X. He, Q. Yin, Z. Zhang, J. Shi and Y. Li, *ACS Nano*, 2011, **5**, 9788–9798.
21 X. Li, B. Cho, R. Martin, M. Seu, C. Zhang, Z. Zhou, J. S. Choi, X. Jiang, L. Chen, G. Walia, J. Yan, M. Callanan, H. Liu, K. Colbert, J. Morrissette-McAlmon, W. Grayson, S. Reddy, J. M. Sacks and H.-Q. Mao, *Sci. Transl. Med.*, 2019, **11**, eaau6210.
22 J. Lim, M. S. K. Chong, J. K. Y. Chan and S.-H. Teoh, *Small*, 2014, **10**, 2495–2502.
23 A. Gefen and B. Dilmoney, *Technol. Health Care*, 2007, **15**, 259–271.

24 M. Sun, M. Wang, M. Chen, F. Dagnaes-Hansen, D. Q. S. Le, A. Baatrup, M. R. Horsman, J. Kjems and C. E. Bünger, *Acta Biomater.*, 2015, **18**, 21–29.
25 M. Bartnikowski, T. R. Dargaville, S. Ivanovski and D. W. Hutmacher, *Prog. Polym. Sci.*, 2019, **96**, 1–20.
26 J. K. Jadapalli, G. W. Wright, V. Kain, M. A. Sherwani, R. Sonkar, N. Yusuf and G. V. Halade, *Am. J. Physiol.: Heart Circ. Physiol.*, 2018, **315**, H1091–H1100.
27 Y. Yang, D. Pan, K. Luo, L. Li and Z. Gu, *Biomaterials*, 2013, **34**, 8430–8443.